# Observations of the Distribution of Ice in Hurricanes

R. A. BLACK

*NOAA/Atlantic Oceanographic and Meteorological Laboratory, Hurricane Research Division, Miami, FL 33149*

J. HALLETT

*Desert Research Institute, Atmospheric Sciences Center, University of Nevada System, Reno, NV 89506*

(Manuscript received 2 January 1985, in final form 21 November 1985)

ABSTRACT

Observations of the type and distribution of particles above the 0°C isotherm in three Atlantic hurricanes are presented. Supercooled drops, graupel, columns and aggregated snowflakes were observed. The supercooled drops were found only in convective updrafts stronger than 5 m $s^{-1}$, but not all updrafts > 5 m $s^{-1}$ contained appreciable liquid. Graupel was found in all updrafts at temperatures < −2°C, and small columns were sometimes found in downdrafts. Nonconvective rainbands contained 15–30 $L^{-1}$ of snow composed of columns and what appeared to be large aggregates. Other stratiform regions contained 1–15 $L^{-1}$ of medium and large aggregates; columns were occasionally found there also but only within about 15 km of convection. Hurricane convection is almost completely glaciated at the −5°C level. It is suggested that the ice particles observed at 6.0 km inside the convection result primarily from downward mixing on both sides of the eyewall updraft of ice formed in the convective areas at higher, colder levels. The ice in the stratiform areas is believed to have fallen from the high-level (6 km and higher) eyewall outflow.

## 1. Introduction

The role of ice in the dynamic structure and evolution of hurricanes is not well understood. In natural cloud systems, ice particles may nucleate on atmospheric aerosols (primary nucleation), through collisions between ice particles, or during graupel growth (secondary nucleation). Measurements of natural ice nuclei have been made at many locations, including the tropics, by numerous researchers using a variety of techniques (Pruppacher and Klett, 1978, p. 241–248). In unpolluted air, these measurements have consistently found low concentrations (<1 $L^{-1}$) of natural ice nuclei active at temperatures warmer than −15 to −20°C. High concentrations of ice at temperatures warmer than those at which large numbers of natural ice nuclei are active can be explained either by secondary nucleation or advection of ice formed elsewhere at colder temperatures. Two possible mechanisms for introducing ice into clouds are entrainment of ice from clouds formed earlier at the same place (Keller and Sax, 1981) and natural seeding of growing clouds with ice falling from a higher, upwind cirrus layer through the cloud top (Heymsfield et al., 1979).

The effect of ice microphysics upon the dynamic structure of hurricanes is being studied with the aid of numerical hurricane models. Lord et al. (1984) developed a model that parameterizes the ice processes by applying somewhat arbitrary linear conversion rates as functions of temperature and saturation between liquid, graupel, and snowflakes. Their results indicate that the presence of ice influences the structure of the storm by maintaining mesoscale downdrafts near the 0°C isotherm over wide areas outside the eyewall. To include more realistic ice-phase microphysics in dynamic models, it is necessary to know the range of particle types, concentrations, and sizes, as well as the sources of natural ice in hurricanes. Furthermore, since the nucleation and growth of ice particles can invigorate cloud growth through the release of additional latent heat and may possibly affect hurricane intensification, it is important to measure the number and shape of the ice particles along with the supercooled water content.

Early observational studies of the precipitation in hurricanes were conducted in the regions warmer than 0°C (Ackerman, 1963). These studies revealed that the liquid water content of hurricane clouds was much lower than the adiabatic value, presumably because of rainout. This result was confirmed as part of a study by Jorgensen and Willis (1982) that used considerably improved instrumentation. In spite of the lack of microphysical observations at temperatures colder than 0°C in hurricanes, the postulated existence of large amounts of supercooled water in hurricane convection formed the basis for Project STORMFURY, a hurricane modification project conducted in the 1960s (Willoughby et al., 1985). The only previously published study on tropical cloud systems for which ice particle image data were collected was the Winter

Monsoon Experiment (WMONEX). These data (Churchill and Houze, 1984) were gathered at about 7.8 km altitude (about −17°C) in both the convective and stratiform regions of tropical oceanic cloud clusters. In convective regions, they found only rounded particles (presumably graupel), while in stratiform regions, columns, branched crystals and aggregated snowflakes were found. The altitudes at which these data were gathered were higher, and the temperatures were colder than in this study.

This study presents the first attempt at a comprehensive description of the complex microphysical structure of hurricane convection above the 0°C isotherm. We will present the data in terms of its relation to the eyewall, rainbands[1], stratiform areas, and storm asymmetry to better infer the origins and transport of the ice in the hurricane. In particular, the observations were aimed at examining convective areas of the storm where supercooled water might occur, as such regions have the potential for the release of the latent heat of fusion when seeded with ice or ice nuclei. The data presented here were gathered with the NOAA WP-3D aircraft in three Atlantic hurricanes: Ella (1 September 1978), Allen (5 and 8 August 1980), and Irene (26 September 1981). Ella and Allen were mature, well-organized storms, while Irene was not so well organized and comparatively weak. The temperatures at which good data were obtained in these hurricanes are about −5°C. The microphysical data from Allen and Irene are particularly noteworthy because of the great volume of high-quality particle images gathered at altitudes above the 0°C isotherm. As discussed later, Allen on 5 August was much different in radar appearance from Allen on 8 August, and Irene had only a strong rainband without an eyewall.

Section 2 presents descriptions of the instruments and analysis procedures. Representative observations from Hurricanes Ella, Allen and Irene are described in sections 3–6. These sections illustrate major microphysical features that were observed on many occasions in these storms. The discussion and conclusions are presented in sections 7 and 8.

## 2. Instrumentation and data analysis

### *a. Instrumentation*

The NOAA WP-3D carries a full complement of meteorological sensors, cloud physics instrumentation and digital radar. The cloud physics instruments package comprises the two-dimensional (2-D) optical array probes manufactured by Particle Measuring Systems, Inc. (PMS), the PMS Forward Scattering Spectrometer Probe (FSSP) (Knollenberg, 1981, pp. 53–63), a Johnson–Williams (JW) liquid water meter, and a formvar replicator (Hallett, 1976). On the NOAA aircraft, the precipitation probe (2D-P) has a diameter range of 0.2–6.4 mm in 0.2 mm steps, and the cloud probe (2D-C) range is 0.05–1.6 mm in 0.05 mm steps. All three PMS probes were mounted under the left wingtip of the WP-3D with the 2-D probe arms oriented vertically. These same probes were used in a comprehensive study of liquid precipitation from mature hurricanes (Jorgensen and Willis, 1982). Since 1980, the 2D-C has contained the phase-discrimination option, which measures the amount of depolarization caused by particles to identify ice particles. The depolarization option detects approximately 30% of the total number of ice particles present, and <10% of the raindrops greater than 1 mm in diameter (Knollenberg, 1981, p. 58).

The other major cloud physics instrument was a formvar replicator. Particles enter the replicator through a slit and impact upon a film coated with formvar solution, which is dried and then taken up on a reel. The formvar replicator is capable of preserving particles of 0.005–2 mm in diameter, thus enabling an observer to distinguish between water and ice in many instances and also to estimate particle concentrations. Gradual degradation of the performance of the replicator occurs in sustained flight through thick ice clouds because ice and splashed formvar solution eventually obstruct the entrance slit, so that data are not available everywhere along the flight track.

Other instruments used in this study are the Rosemount Total Temperature Probe (model 102) and digitized radar. Rosemount temperature probes are known to underestimate the air temperature by 1–2°C in liquid water clouds (Lenschow and Pennell, 1974). With this caveat in mind, the temperatures given in this paper were corrected only for airspeed effects and can be considered completely accurate only outside liquid water regions. The radar data (Jorgensen, 1984a) consisted of horizontal plan position indicator (PPI) and vertical range-height indicator (RHI) scans obtained with the lower fuselage radar (PPI, 5.5 cm), and the tail radar (RHI, 3.0 cm). The lower fuselage radar data were composited to produce horizontal representations over selected areas of the storm, usually centered on the eye. The method used to create the composite figure (Marks, 1985) emphasizes features that exist for a substantial portion of the composite period, two hours in this case. The PPI scans were made at small (<2°) downward tilt angles, and they represent a typical radar view of the storm near the flight altitude. Vertical cross-sections along the flight track were produced from the tail-radar data.

### *b. Data analysis procedures*

Because of the lack of independent corroborating particle-type data, the 2D-C particle image data were subjectively classified by hand. The 2D-P data were not analyzed as extensively as the 2D-C data. The 2D-

[1] The term rainband is derived from the occurrence of banded radar echoes spiraling around the wind center and does not necessarily imply rain formation at temperatures below 0°C.

TABLE 1. Size ranges of the principal microphysical sensors on the NOAA WP-3D aircraft.

| Instrument | Size range (mm) |
|---|---|
| 1. Formvar replicator | ~0.005–2 |
| 2. Johnson–Williams LWC | < ~0.04 |
| 3. PMS FSSP-100 (Max) | 0.003–0.045 |
| 4. PMS 2D-C | 0.05 –1.60 |
| 5. PMS 2D-P | 0.20 –6.40 |

P data were used only to confirm or deny the presence of large particles and to estimate the concentration of particles with diameters > 1 mm. This procedure was used because of the great overlap of the 2-D probe size ranges (Table 1). A peculiar feature of the 2D-C image data is that in rain, all of the drops > ~ 1 mm in diameter are elongated, with the major axis canted at about 45° to the aircraft motion. That this canting is real was demonstrated in the 1981 data. Between the 1980 and 1981 field seasons, the 2D-C was inverted with respect to its 1980 position, and raindrop images in the 1981 data remained elongated and canted, but the major axis of the image was rotated 90° with respect to the 1980 data. It is interesting that the canted raindrops are asymmetrical about their major axis, with one side flattened as occurs in raindrops > 1 mm diameter falling in still air (Fig. 1). The flattening of these images is about twice as great as expected for raindrops of this size falling at terminal velocity in still air, suggesting that the drops are being additionally deformed in the accelerated airflow around the probe support pylons. Graupel or any other ice images were not canted or deformed in any way. The observed shapes provide an unequivocal means of identifying supercooled raindrops.

The four categories of particle that we found, and the criteria used to identify them are as follows.

1) Canted, elongated images greater than about 0.8 mm were all classified as liquid. Particles with diameters from 0.4–0.8 mm were classified as liquid if the images were rounded and the images were recorded in areas with JW liquid water content (lwc) > 0.1 g $m^{-3}$, temperature > −1°C, or updraft > 1 m $s^{-1}$. Particles of <0.4 mm diameter were always classified as liquid unless the criteria in 4) below were met.

2) Graupel particles were all nearly round images of >0.5 mm diameter located at temperatures < −1°C in areas without updrafts. In updrafts where *JW* liquid water was present, images had to be >1 mm in diameter, rounded, and could not be canted to be considered graupel, in order to avoid confusion with raindrops.

3) A column was an approximately rectangular image whose maximum length was at least twice its minimum length.

4) Snowflakes included all other images since no other regular crystal habits were present in the data. Particles of longest dimension < 0.4 mm were considered to be ice if the JW lwc was <0.3 g $m^{-3}$, the vertical motions did not exceed 1 m $s^{-1}$, and the temperature was < −1°C.

The identification of medium and small graupel from 2-D images is difficult because those particles often look like small rain drops. Consequently, the graupel discrimination was subjectively based upon the visual appearance, JW liquid water, and vertical velocity. In doubtful cases, the particle was assumed to be graupel if the output of the 2D-C phase-discrimination option indicated a strong (level 2 or more out of 8 levels) cross-polarization component to the signal. These criteria appeared to be adequate because the observed low updraft velocities at 50 kPa in hurricanes (Jorgensen et al., 1985) cannot support large particles.

Software for use on a minicomputer was written to compute the 2-D particle sizes according to the equivalent circle diameter of the image, the number concentrations, and water content. Equivalent circle diameter is the diameter of a circle with the same area as the particle. For purposes of this study, the particle sizes were divided into small, medium, and large classes. Small particles were those of diameters from 0.05 to 0.5 mm, medium particles were of 0.5 to 1.05 mm diameter, and large particles were those >1.05 mm in diameter. These classifications are essentially the same as those used by Churchill and Houze (1984).

The 2-D images were examined by computer to eliminate "artifact" images caused by particles that disintegrate within the field of view. Zero-area images were also rejected on the grounds that they were indistinguishable from electronically generated false time codes not associated with cloud particles. Images with the maximum dimension on an edge of the field of view were rejected to eliminate partial images. Images with a gap parallel to the diode array were rejected to eliminate splashes and fragmented ice images. Images

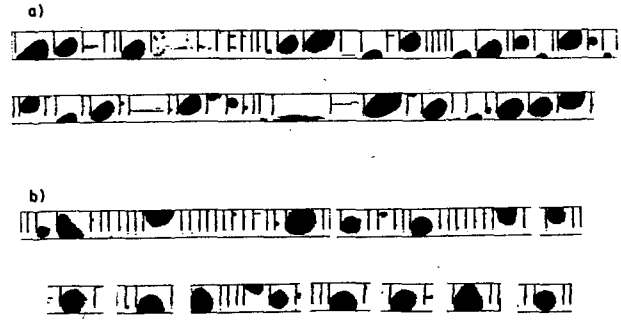


FIG. 1. Raindrop and graupel images taken in Hurricane Irene in 1981. (a) Raindrop images from a pass at 1.5 km (+15°C) on 27 September, and (b) graupel images from 6.2 km (−5°C) on 26 September. Note the elongation and canting in the raindrop images in comparison to the graupel images.

whose temporal separation was not within two standard deviations of the mean separation for the record were rejected to prevent distortion of the concentrations by either any of the numerous small droplets associated with splashes, or the first particle following a long gap without particles. This test assumed that the particle separation times formed an exponential distribution. Streakers, images recorded when liquid water is shed from the probe tips, were eliminated by rejecting images with a maximum extent perpendicular to the diode array > 4 times the parallel extent, 6 times if the image was wholly inside the field of view. Finally, images with an area less than 0.4 times the product of the parallel and perpendicular extents were rejected to eliminate splashes and fragments not rejected by the other criteria.

These tests typically eliminate from 20 to 50% of the original particles recorded by the 2-D probes. Streakers comprised a maximum of 20 to 30% of all images in rain areas, to less than 3% of all images elsewhere. They never accounted for more than 10% of the elapsed time in a 2-D record. Sample volumes, particle number concentrations, liquid water content, approximate ice water content, and 5.5 cm radar reflectivity were calculated only from the acceptable particles. The reflectivity and some of the water content calculations will be presented in a later paper. In addition, all of the images themselves were plotted on a dot-matrix plotter to aid in the interpretation of the computer results.

The formvar data were analyzed with a standard 16 mm projector. Particles that appeared on each frame were counted, sized and identified visually. Timing was fixed by marks placed on the film at known times and the film transport speed was recorded as it was exposed, thus the sample volume for each frame was obtained and the observed particle concentrations were calculated.

## 3. Hurricane Ella—1 September 1978

On 1 September 1978 Hurricane Ella was a mature, moderately well-organized hurricane (Fig. 2a). The storm was over the Atlantic Ocean about 500 km southeast of Cape Hatteras and was moving slowly toward the northwest (Lawrence, 1979). The minimum central pressure and strongest tangential winds as recorded by research aircraft were 95.9 kPa and 50 m $s^{-1}$, respectively. Following the terminology of Willoughby et al. (1984), Ella had a closed, circular eye and a well-defined principal rainband that extended from about 50 km on the west of the eye around the south side to 15 km on the north of the center. Most of the intense radar echoes in Ella were southeast of a line through the center and oriented from southwest to northeast. The aircraft flight pattern consisted of radial legs at constant radar altitude passing through the radar eye and symmetrically arranged in direction. This flight pattern, as well as those for all other high altitude hurricane research missions, was specified before the flight and was followed strictly throughout the mission. Several radial penetrations from the principal rainband to the eye were completed.

### *a. Principal rainband pass and part of eyewall*

The first penetration (1851:00–1857:00; all times GMT) of Ella was at an altitude of 6500 m and a temperature of about −9.0°C. The radial leg began on the southwest side of the storm and intersected both the principal rainband and the eyewall. On this pass, no detailed temperature, JW lwc, vertical velocity, or position data are available because the original data were inadvertently destroyed during the flight, but good formvar data were obtained. In both the principal rainband and the eyewall, the formvar analysis revealed the presence of either graupel or snowflakes of 0.5–2.0 mm diameter in concentrations up to 100 $L^{-1}$ and ice water contents up to about 3 g $m^{-3}$, assuming an ice particle density of 0.1 g $cm^{-3}$. Ice particle concentrations of about 2 $L^{-1}$ were observed in the region between the principal rainband and the outer edge of the eyewall.

Although the formvar data showed primarily snow and graupel, some unrimed columnar crystals (Fig. 3) were found in the rainband at about 1852:00. The identification of these columnar ice crystals is significant because columnar ice grows only at temperatures near −4°C, yet there was little supercooled cloud water where the columns were found. Thus, it is inferred that the columns were grown at a warmer, lower level and were carried up to the flight level.

The PMS probe data (Fig. 4) corroborated the formvar record, with 2D-P (graupel) particle concentrations of 1–19 $L^{-1}$. In the rainband itself, the 2D-P particle concentration averaged 11 $L^{-1}$ from 1851:35 to 1853:00, with a maximum of 19 $L^{-1}$ at 1852:20. Outside the rainband from 1853:30 to 1855:40, the 2D-P concentration averaged 1–2 $L^{-1}$. Small particle concentration data observed by the 2D-C probe ranged from about 5 to over 100 $L^{-1}$, all of which the replicator showed to be graupel particles of snowflakes. The 2D-C concentration in the rainband averaged 40 $L^{-1}$ with several concentration spikes > 100 $L^{-1}$ and a maximum of 172 $L^{-1}$ at 1851:50. Outside the rainband, the 2D-C concentration averaged 1 $L^{-1}$. Most of the large particles appeared to be snowflakes.

Cloud droplet data gathered near the eyewall with the replicator revealed droplets in all size categories (Fig. 5). These spectra illustrate the wide variability of the droplet size distribution in these clouds, which indicates that strong mixing took place in them. Regions containing cloud water droplets were identified both at the inner edge of the rainband and just before the aircraft entered the eye at about 1857:00. The cloud droplets were found in low concentrations (<100 $cm^{-3}$)

over about 0.5 km in the rainband, and in somewhat higher concentrations in the outer portion of the eyewall. In this portion of the eyewall, the cloud liquid water content was ~0.5 g m$^{-3}$ and the ice water content was ~0.25 g m$^{-3}$. It is interesting that the 0.5 Hz FSSP cloud droplet size distributions and number concentrations showed wide variability and counts in all parts of its size range. In all of the regions where the replicator

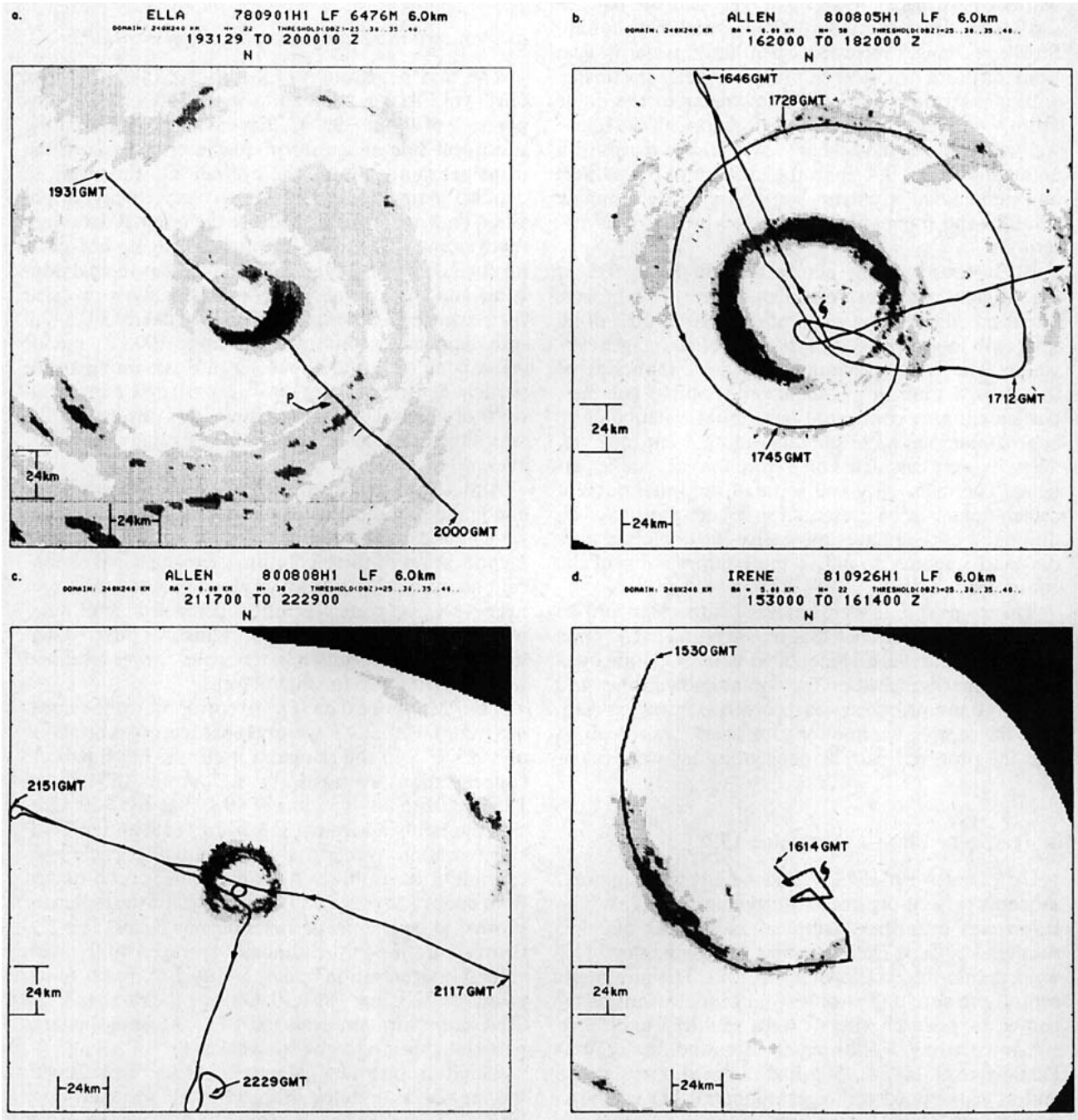


FIG. 2. Horizontal radar composites at 5.5 cm of the three hurricanes involved in this study. The domain of these composites is 240 km square, the altitude is about 6.0 km and the reflectivity levels are at 25, 30, 35 and 40 dBZ.

(a) Hurricane Ella (1 September 1978) during the traverse from 1931–2000 GMT. The principal rainband is marked "P."
(b) Hurricane Allen (5 August 1980) near the time of the circumnavigation of the storm from 1620 to 1820 GMT.
(c) Hurricane Allen (8 August 1980). The pass discussed in the text penetrated the eyewall on the west side.
(d) Hurricane Irene (26 September 1981) during the rainband circumnavigation of 1530–1614 GMT. The radial pass of 1408–1418 GMT traversed an intense core near the downwind edge of the raindband.

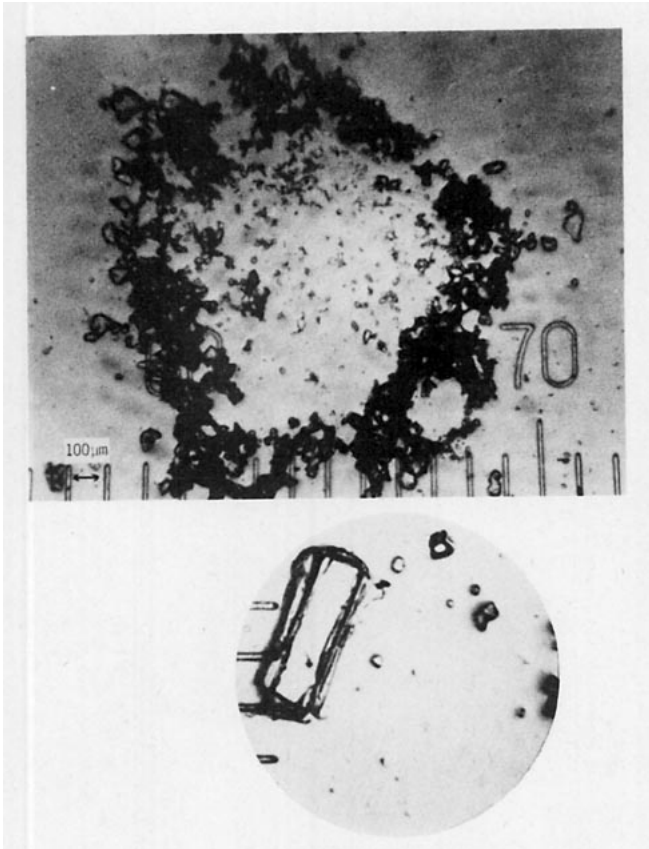


FIG. 3. Formvar replica of graupel and unrimed column sampled in the rainband of Ella at about 1852 GMT.

recorded cloud droplets, graupel or snowflakes were also present in concentrations of about 0.2 $L^{-1}$.

*b. Eyewall penetration*

The formvar replicator was inoperative during the eyewall penetration (1932:00–1950:00) and subsequently, but the PMS data and the meteorological flight data were recorded as the aircraft flew out of the eye radially toward the southeast. This traverse occurred at the coldest temperature (~ −7°C) from which 2-D data are available. The variations of temperature, JW liquid water, vertical velocity, and 2-D concentration as a function of time are shown from the eye to the principal rainband (Fig. 6). Note the downdrafts that occurred on the inside edge of the eyewall at 1940:30 and 1942:30. These downdrafts occurred in air that was essentially clear, without detectable cloud liquid water. The 12 m $s^{-1}$ updraft peak at 1940:10 in the northwest eyewall only had 0.5 g $m^{-3}$ JW lwc, but the 3–4 m $s^{-1}$ updraft in the southeast eyewall centered at 1942:45 contained about 2.0 g $m^{-3}$ of JW liquid water. The low JW lwc in the 1940:10 updraft might be explained by the presence of precipitation-size particles there, but no particle data were available.

The eyewall updraft at 1942:45 contained only 2 $L^{-1}$ large (>1.05 mm diameter) supercooled raindrops and graupel (2D-P), but the 2D-C concentration varied from 20 to 75 $L^{-1}$ and increased rapidly as a downdraft on the outer edge of the eyewall was approached. At the inner edge of the updraft, the 2D-C ice particle concentration was <5 $L^{-1}$, but the proportion of ice particles in the 2D-C images increased to 100% by 1943:00. The downdraft in the southeast eyewall reached 3 m $s^{-1}$ at 1943:50. The peak 2D-P concentration of 36 $L^{-1}$ was encountered at 1943:30 in this downdraft, where most of the larger particles appeared to be graupel. At the same time, the 2D-C concentration was well over 400 $L^{-1}$, peaking at about 680 $L^{-1}$. The poor quality of many of the 2D-C images renders these concentrations doubtful, however. Many of the smaller (2D-C) images in the concentration peak appeared to be columnar, similar to the columns recorded by the formvar replicator earlier. After about 1944:00, all of the particles were graupel or snowflakes. The 2D-P concentration outside the eyewall was 10–20 $L^{-1}$, while the 2D-C concentration was 20–50 $L^{-1}$.

Although specific observations were not made, Ella had substantial electrical activity, with lightning flashes observed at about 30-second intervals, during the eyewall penetrations (V. Keller, private communication, 1985).

## 4. Hurricane Allen—5 August 1980

Hurricane Allen was a mature, well-organized storm on 5 August 1980 and was characterized by an extensive cirrus canopy that covered much of the storm circulation (Lawrence and Pelissier, 1981). On 5 August, Allen had an outer eyewall 70 km in diameter surrounding a smaller, dissipating inner eye 20 km in diameter. The average minimum sea level pressure was about 95 kPa and the maximum tangential wind was approximately 60 m $s^{-1}$ (Willoughby et al., 1982). Allen was located in the Caribbean Sea about 150 km south of Hispanola (Haiti) and was moving west at about 10 m $s^{-1}$. Allen's convection was distributed in a complete circular eyewall, but the most intense radar echoes were in the north and northwest sectors of the storm. Upon

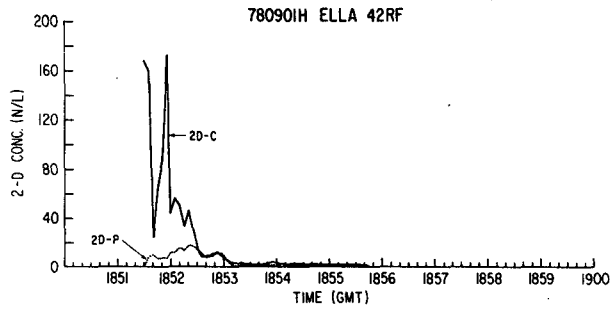


FIG. 4. 2-D particle number concentration measured during the first radial pass through Ella.

arrival, the aircraft made two perpendicular radial passes at maximum altitude (5.5–6.3 km) through the eyewall to beyond the principal rainband and back. Then it began flying radial penetrations and exits along the northwest–southeast azimuth at various altitudes. After flying the radial pattern for about 6 hours, the aircraft completed a downwind circumnavigation of the storm at 6 km in the principal rainband. Within each radial leg and the circumnavigation, the radar altitude was constant. No lightning was observed, but most of the flight took place during daylight hours.

A radar composite made on this day (Fig. 2b) reveals the main features of the convection in the outer eyewall and principal rainband at 6.0 km altitude. Note, in particular, the very strong reflectivity of the outer eyewall, the relatively weak reflectivity of the rainband, and the symmetry of the eyewall reflectivity compared with the pronounced asymmetry in Ella. The convection in the inner eyewall was relatively weak and is not clearly depicted in the radar composite at 6.0 km. In the following discussion, we describe traverses of weak and strong portions of the outer eyewall, and then the

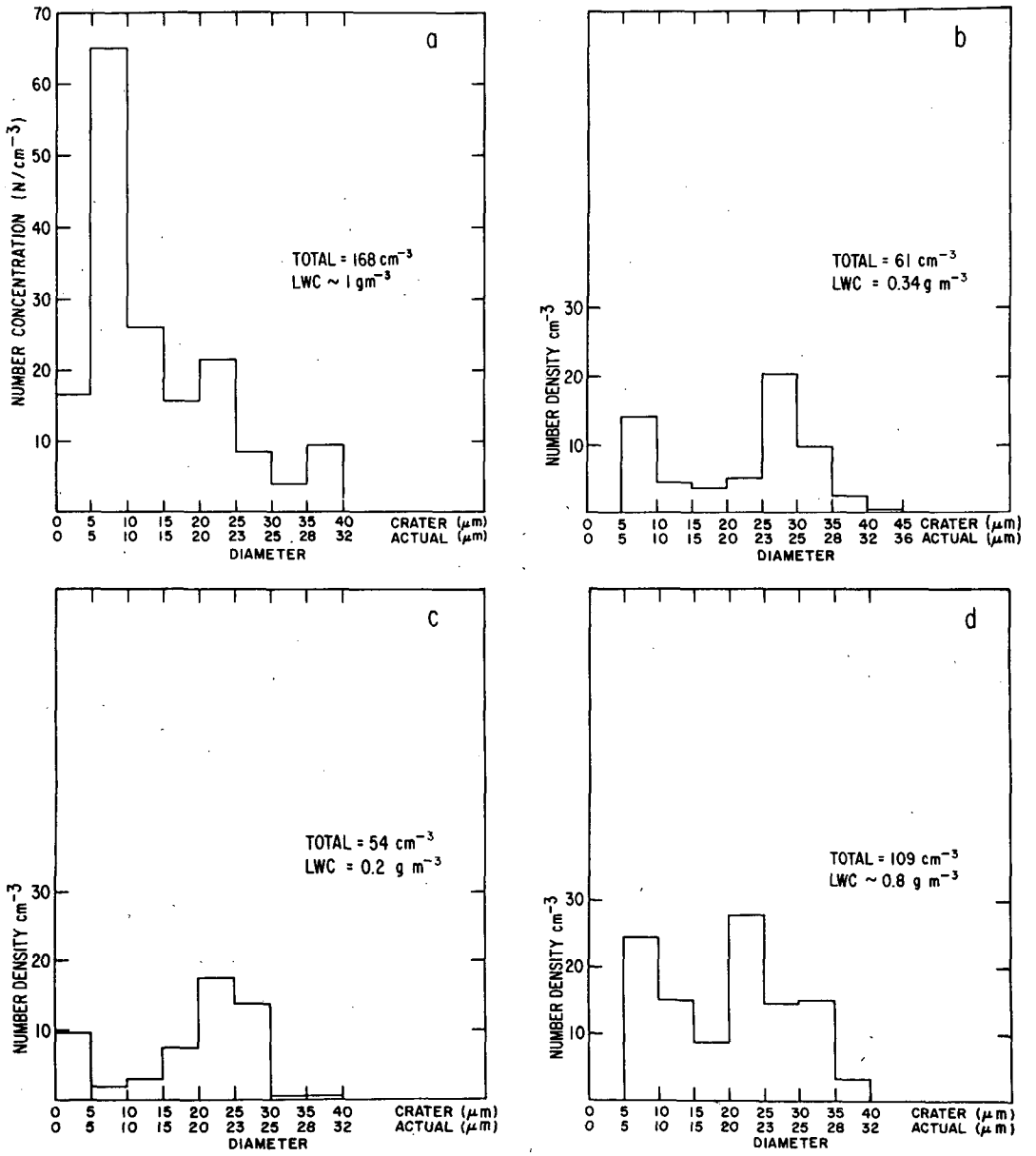


FIG. 5. Formvar cloud droplet size spectra in the rainband and eyewall of Hurricane Ella. (a) At inner edge of rainband near 1852:15. (b) Outer edge of eyewall near 1856:00. (c) As in (b), but near 1856:10. (d) As in (c), but at about 1857:00.

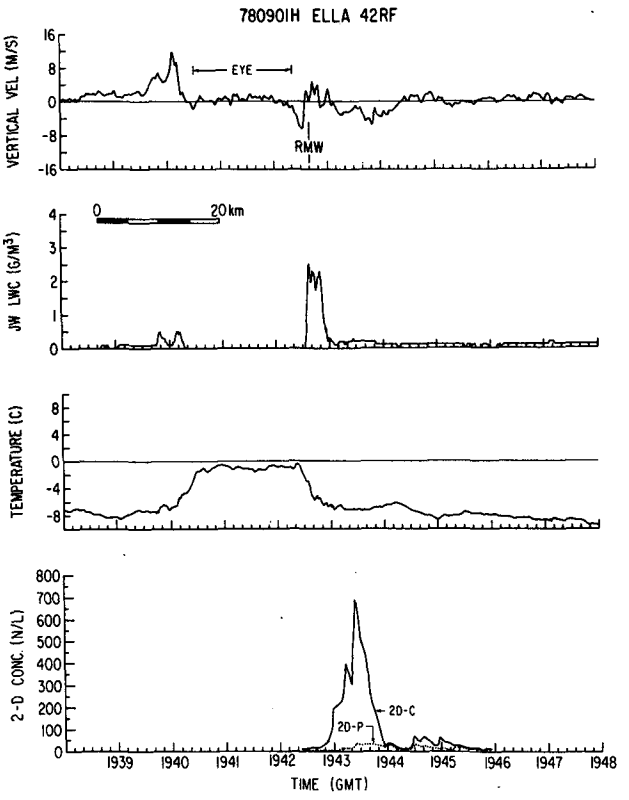


FIG. 6. Vertical velocity, JW cloud liquid water content, temperature, and 2-D particle concentration for the rainband and eyewall pass from 1930–1950 GMT in Ella.

circumnavigation. The term eyewall will always refer to the outer eyewall of Allen on this date.

### *a. Traverse of weak part of eyewall, 5 August 1980*

Figure 7 shows the variations of temperature, vertical wind speed, JW liquid water content, and 2-D concentration measured as the aircraft penetrated a typical weak updraft in the eyewall on the inbound leg from the northwest side from 1432–1442. This portion of the eyewall was characterized by 2–4 m $s^{-1}$ updrafts and only 0.2–0.4 g $m^{-3}$ cloud liquid water content before the aircraft crossed the 0°C isotherm, and 1.0 g $m^{-3}$ afterward. The eyewall horizontal temperature gradient on this radial was weaker than that on the north radial only 30 minutes later. This portion of the eyewall had fewer particles in its updrafts than occurred either in its downdrafts or in the outer stratiform region, and the average particle concentration on this penetration was less than in the strong north eyewall. The 2-D concentrations were not well correlated with the vertical wind speeds.

An examination of the JW liquid water content and the vertical wind shows that between 1436:30 and 1437:00, the updraft reached nearly 4.0 m $s^{-1}$ but the JW liquid water content never exceeded 0.4 g $m^{-3}$ until about 1437:30, when the temperature in the updraft had climbed above 0°C. This behavior is consistent with a glaciated updraft because penetrations at temperatures warmer than 0°C had liquid water contents $> 1$ g $m^{-3}$ in 4.0 m $s^{-1}$ updrafts (e.g., see 1453:40 in Fig. 8). Again, there was a downdraft on the inside edge of the eyewall at 1437:40.

The outer (colder) portion of this traverse was almost totally glaciated (Fig. 7), but the quantity of ice decreased rapidly as the aircraft entered regions warmer than 0°C. The 2D-C images observed between 1436:30 and 1437:00 indicate that ice particles existed close to the 0°C isotherm.

A comparison of the images recorded radially outside the eyewall convection with those in the eyewall reveals substantial differences in particle type between the two regions. Some particles observed outside the eyewall exhibited the columnar and needlelike combination shapes characteristic of growth near −4°C at water saturation. These particles were mixed with the more usual assortment of snowflakes and graupel-like shapes, but the columnar forms seemed to be the most numerous at certain points outside the major convective cores. Many of the particles outside the eyewall were larger than about 0.5 mm, and large particles made up a greater percentage of the particle concentration. The particle mix outside the eyewall resulted in flatter particle spectra there, in contrast with the eyewall, where many new particles were continuously formed in the updrafts.

### *b. Strong eyewall traverse, 5 August 1980*

The next leg extended out from the eye toward the northwest. On this traverse, the aircraft encountered the widest, strongest updraft (12 m $s^{-1}$ peak, 7 m $s^{-1}$ average) measured in Allen near the 0°C isotherm. The variations of temperature, vertical wind speed, JW liquid water content, and 2-D concentration (Fig. 8) clearly show the entrance into the main eyewall at 1456:00. The JW spike at 1453:30 is from the remnants of the inner eyewall. As expected, the JW peak is well correlated with the active updraft at these warm temperatures.

In the main updraft, the medium and large particles were primarily raindrops with a concentration of 20 $L^{-1}$. A few of the particles on the edge of the main updraft appeared to be well-defined graupel (Fig. 8) on the basis of irregular, uncanted outline in the 2D-C images, and depolarization signal. This graupel indicated that the temperature of this part of the updraft was colder than 0°C and that strong lateral mixing had occurred. As the aircraft entered the eyewall downdraft farther out from the eye, the water drops disappeared and were replaced by graupel and other small ice. The transition between essentially all water and all ice particles in this instance was very sharp, and occurred in <100 meters along the flight track. At 1457:30, the aircraft encountered a 4 m $s^{-1}$ downdraft and the par-

ticle concentration abruptly increased to about 130 $L^{-1}$, with 20 $L^{-1}$ identified as medium and large ice.

The particle size distribution also changed shape. In locations where particles are growing in diameter, the size spectra of cloud particles (0.01–3 mm) are steeply sloped because of the rapid growth of small particles and the fallout of the precipitation sized particles. In the main updraft, the JW liquid water content exceeded 2 g $m^{-3}$, but the 2D-C size spectra were relatively flat, indicating that few of the small particles had the opportunity to grow large enough to be detected by the 2D-C before being collected by precipitation particles. However, in the downdraft, the spectra were steeply sloping with many small particles, and the JW liquid water content was <0.2 g $m^{-3}$. In this case, the individual size spectra showed many particles < 0.5 mm diameter and some particles > 1.0 mm diameter, but relatively few particles that were from 0.5–1.0 mm diameter. Nearly all of the images of 0.5 mm diameter or larger were graupel particles. The steeply sloping particle size distribution in the downdraft indicated that the aircraft was near a region of rapid particle formation.

As the aircraft flew farther away from the eyewall, no additional updrafts or downdrafts were encountered. The particles had flat size spectra and were mostly aggregated snowflakes. Particles of this type (Fig. 8) were abundant in all stratiform portions of Hurricane Allen. The abundance of these particles is shown clearly in the circumnavigation of the rainband.

*c. Principal rainband circumnavigation, 5 August 1980*

From 1721:00 to 1750:00, the aircraft flew a circumnavigation of the storm downwind in the principal

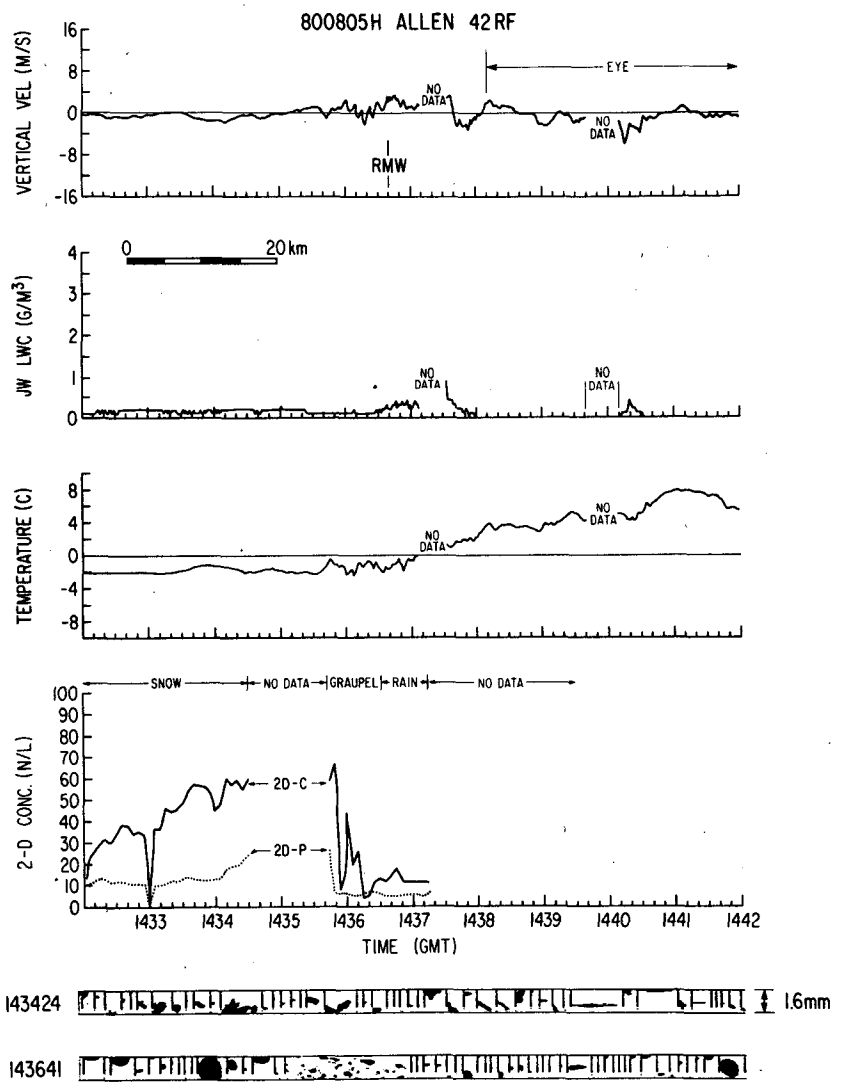


FIG. 7. As in Fig. 6 but on the weak side eyewall penetration of Allen of 5 August 1980. The particle images were taken with the 2D-C at the indicated times.

rainband at the 6.0 km (−5°C) level. This rainband had a diffuse appearance on radar and was characterized by stratiform precipitation with uniform reflectivity at about 25 dBZ. The radar "brightband" was often present at 4.5–5 km and few active convective cores reached the 6 km level. The vertical winds during most of this traverse seldom exceeded ±1 m $s^{-1}$, and the JW liquid water content was greater than the background noise level (0.1–0.2 g $m^{-3}$) only once. This traverse provided a good azimuthal average of particle types and concentrations at the −5°C level in stratiform areas.

Throughout the relatively nonturbulent portion of the rainband, the particles were mainly a combination of aggregated snowflakes, graupel, and columns. The number concentration of these particles was higher, 20 $L^{-1}$ as opposed to 1–10 $L^{-1}$ between the principal rainband and the eyewall. At 1746:00, the aircraft encountered a 2.0 m $s^{-1}$ downdraft followed by a turbulent updraft that peaked at 6.0 m $s^{-1}$. Particle concentra-

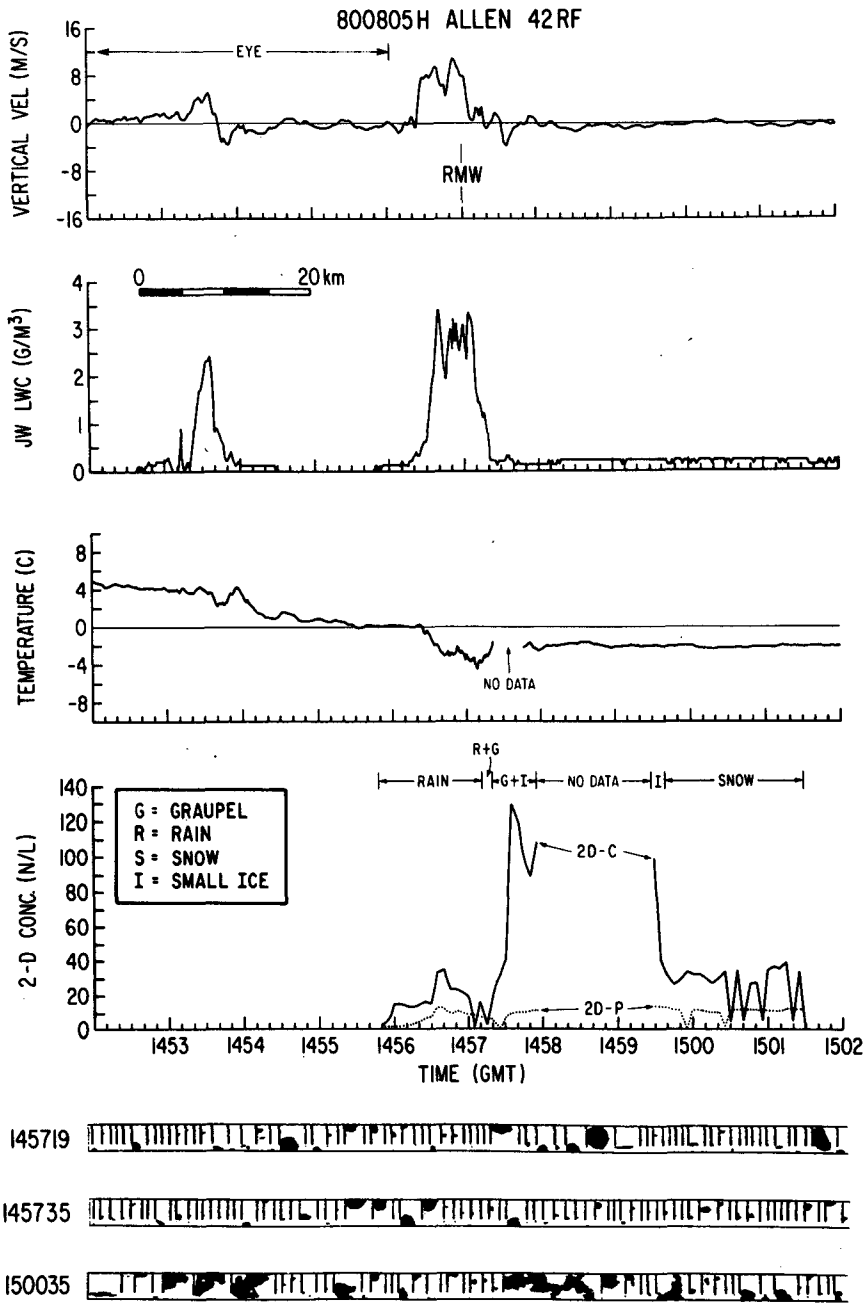


FIG. 8. As in Fig. 7 but for the strong side eyewall traverse of Allen.

tions in this area followed the same pattern as in the eyewall: high concentrations in the downdraft areas and low concentrations in the updraft (Fig. 9). Significantly, nearly all of the particles > 0.5 mm diameter in the updraft were identifiable as graupel. The ice particles had a concentration of 10 $L^{-1}$ compared with a total particle concentration of 20–30 $L^{-1}$. The particles appeared to be millimeter diameter graupel and somewhat smaller irregular ice, a result consistent with growth by rime accretion in an updraft. In the nearby downdraft, the millimeter graupel as well as many smaller particles were present in greater quantities. The ice in the rainband updraft at −5°C is in direct contrast to the eyewall updrafts at 0 to −1°C, where very few (if any) of the particles were ice.

## 5. Hurricane Allen—8 August 1980

By 8 August 1980, Hurricane Allen had moved into the southern Gulf of Mexico west of Cuba. Visible satellite photographs show that its cirrus canopy was much less dense and not so widespread (Lawrence and Pelissier, 1981). The storm's eye was about 25 km in diameter, and the eyewall was completely isolated from

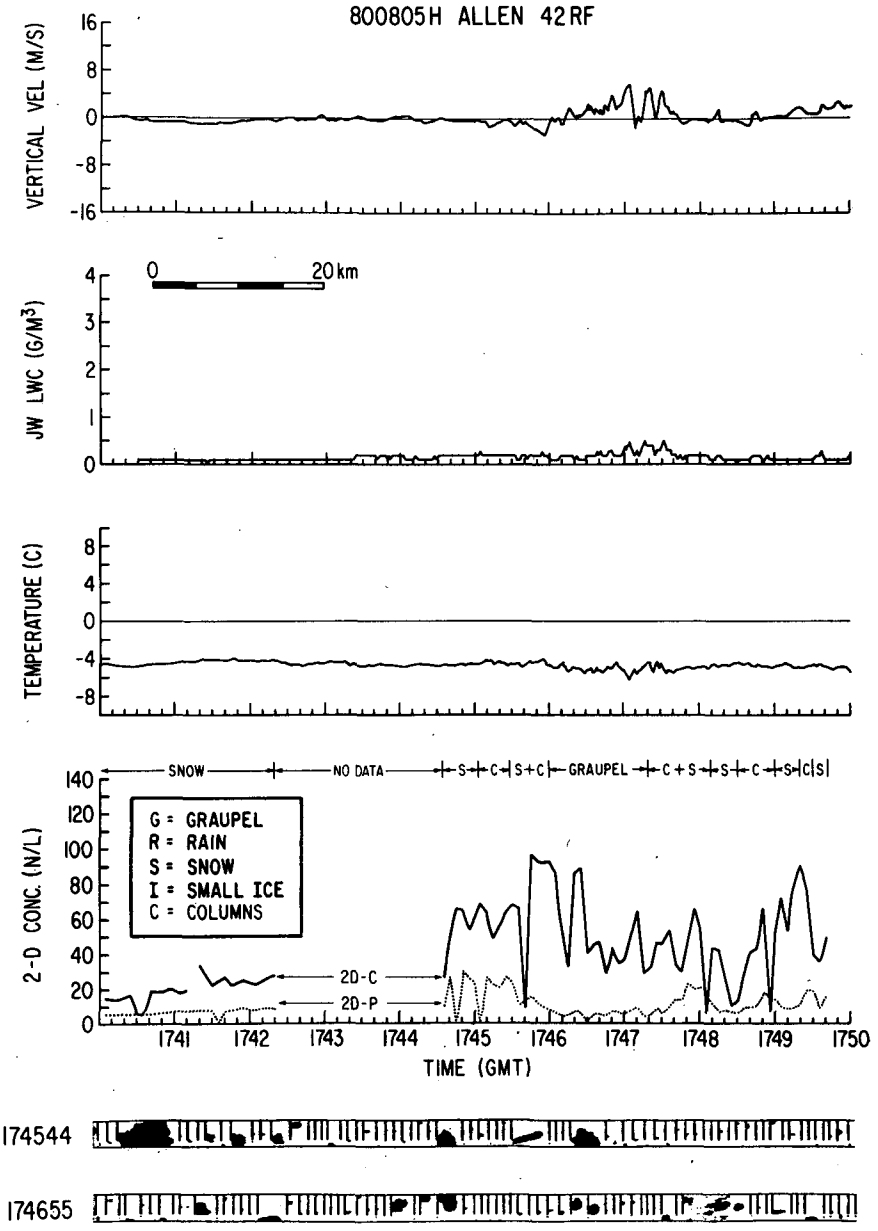


FIG. 9. As in Fig. 7 but for the end of the circumnavigation of Allen's stratiform rainband at 6.0 km altitude.

the nearest rainband (part of which is visible in Fig. 2c). This band was about 75 km from the eyewall at its closest point. The central pressure on this date was about 93 kPa and the maximum tangential wind was about 60 m $s^{-1}$. The aircraft flew cross patterns through the eye at constant radar altitude, similar to those on 5 August, but the radial passes were more symmetrically distributed. This day also had the only lightning observed in Allen, but again, most of the high altitude penetrations occurred in daylight.

Figure 10 presents the variations of temperature, vertical wind speed, JW liquid water content, and 2-D concentration for one pass through the eyewall. This pass penetrated a relatively strong, 5 km wide updraft embedded in the eyewall. During the portion of the pass from 2153:00 to 2157:00, no significant up- or

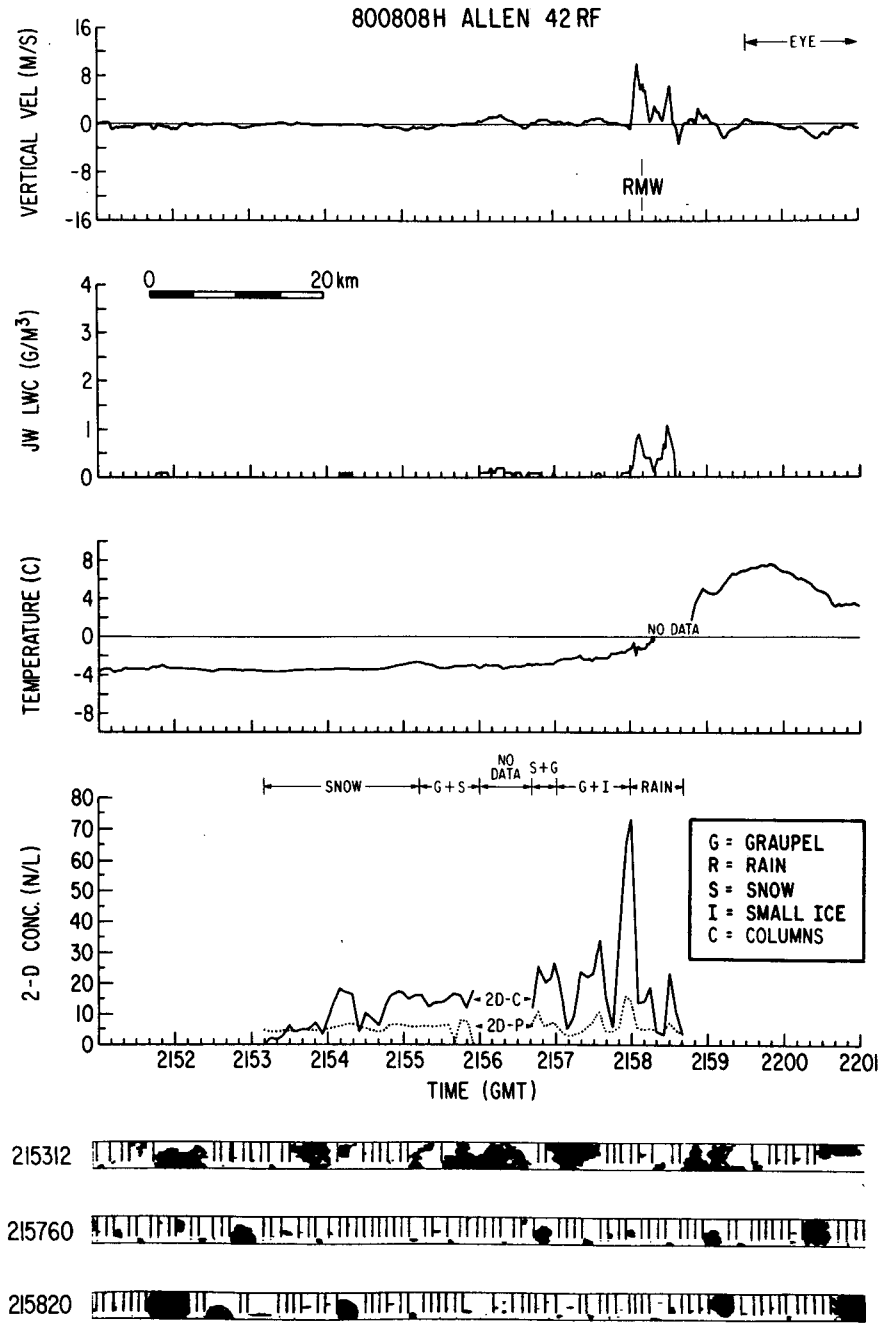


FIG. 10. As in Fig. 7 but for the traverse of Allen's eyewall on 8 August 1980.

downdrafts were encountered and the 2D-C particle concentration was about 5–10 $L^{-1}$. These particles were columns, large snowflakes and graupel (Fig. 10). By 2157:00, the particles were mostly graupel, with variable concentrations averaging 15–20 $L^{-1}$. Just before the updraft, there was a hint of a downdraft in the vertical velocity profile. At this time, the 2D-C number concentration increased to almost 160 $L^{-1}$. The particles appeared to be graupel with small needles or columns. As on the other passes, there was a downdraft on the inside edge of the eyewall.

The peak eyewall updraft of 10 m $s^{-1}$ occurred at 2158:00 and lasted for about 15 s (2 km). The abrupt rise of the JW liquid water content coincident with both a strong updraft and a temperature near 0°C suggests that the particles were liquid. All of the particles observed in the central core of the updraft appeared to be water, but some particles that may have been ice were observed inside the eyewall in areas with weak upward vertical velocities of 1–3 m $s^{-1}$ (at about 2158:20 in Fig. 10). No other ice particles were observed, although the updraft continued for another 2 km until 2158:30. At 2201:00, a lightning strike disabled the PMS probes. The aircraft was at the inside edge of the eyewall about 1.5 km away from the eyewall updraft at the time, but it had not yet entered clear air.

## 6. Hurricane Irene—26 September 1981

Irene was more convective and not so well organized in comparison with Allen and Ella. On 26 September 1981, Irene was about 1500 km east of Puerto Rico and moving northwest at about 7–8 m $s^{-1}$. Irene's maximum surface winds were about 45 m $s^{-1}$, and the estimated minimum surface pressure was about 96.5 kPa. Irene was highly asymmetric, with a strongly convective principal rainband that spiraled toward the wind center from the outer regions and no eyewall (Fig. 2d). This band had some of the convective characteristics of an eyewall, but unlike the eyewall of Allen, the temperature at 6.2 km was −2 to −5°C instead of +1°C. No lightning was observed in Irene. We will discuss, in some detail, the radial pass through the principal band and the partial downwind circumnavigation in the principal band. These passes encountered some of the strongest vertical winds and the highest reliable 2D-C particle concentrations observed above the 0°C isotherm in an Atlantic hurricane. These passes are presented both in order to highlight the particle types found above the 0°C isotherm, and to compare the findings in Allen with the strong convective rainband of Irene.

The radial variations of JW liquid water content, vertical wind and temperature (Fig. 11) show that the strongest updraft had maximum vertical velocities of 10 m $s^{-1}$ and 2.0 g $m^{-3}$ cloud liquid water at −2°C. The large 2D-C concentration increase in the downdraft area occurred where the particle phase changed from primarily liquid to solid. Again, as in the Allen case, the transition between all supercooled water to all ice occurred quickly, in <150 m along the flight track. The 2D-P also showed a great increase in number concentration at about 1415:10.

There were 2–3 large (>1.05 mm diameter) particles per liter in the updraft out of 6–8 $L^{-1}$ total particles, based upon the 2D-P spectra. Some of these particles (Fig. 11) are graupel, and the rest were supercooled raindrops. However, the central core of this updraft contained only supercooled raindrops.

In the downdraft, the 2-D probes revealed a great number of particles, many of which were quite close to the lower resolution limit of the 2D-C. Some of these particles were columns, which implies a growth temperature of −4°C. From 1415:00 to 1416:30, the 2D-C concentration peaked at over 200 $L^{-1}$. Most of these particles are clearly identifiable as ice. These particles were generally 0.5 mm diameter or smaller, with relatively few larger ones. Graupel was also much in evidence at this point. The 2D-P concentration averaged about 5 $L^{-1}$ in the downdraft and peaked at 20 $L^{-1}$. The 2D-C imaging revealed that nearly all of the particles observed with the 2D-P were ice. At larger radii on this pass, a small amount of formvar data were collected. These data corroborated the 2D-C data and showed primarily unrimed ice particles and a few columns.

### *a. Circumnavigation*

From 1530 to 1600 GMT, the aircraft flew down the length of the rainband at altitudes about 300 m higher than the radial pass at temperatures near −5°C. The strength of the convection in this rainband was similar to that in the eyewall of Allen. We believe that the conditions in Irene's principal rainband are similar to those in an eyewall at a temperature of −5°C. During the circumnavigation, the aircraft encountered a long series of convective updrafts (Figs. 12 and 13). The larger updrafts were 5–10 km wide. Nearly all of them contained graupel particles as well as liquid water. Only the updrafts at 1535:30, 1539:00, and 1544:00 had any medium or larger supercooled liquid water drops, and these were less than half as numerous as graupel particles of similar size. Except for the updraft of 1535:30, the only other updraft with a JW liquid water content > 0.5 g $m^{-3}$ was at 1539:00, with a peak JW liquid water content of about 0.7 g $m^{-3}$.

The 2-D particle concentration along the circumnavigation showed the usual pattern of relatively low particle concentrations in the strong updrafts and substantially higher concentrations in the downdrafts. Between the start of the circumnavigation at 1527:00 and 1531:13, the 2D-P measured 8 $L^{-1}$ and the 2D-C showed 100 $L^{-1}$. The particles consisted of graupel, snow, and small ice particles, but the 2-D particle number concentrations gradually decreased downwind of this area.

Between 1531:30–1545:00, the 2D-P averaged 2–3 $L^{-1}$ and the 2D-C measured 30–40 $L^{-1}$. No liquid water was observed during the circumnavigation except for short periods at 1535:30, 1537:30, 1539:00, 1541:30, 1541:50, and 1544:30. Closely spaced updrafts were encountered until 1545:00, and all of the supercooled water was found either inside or immediately downwind of >5 m $s^{-1}$ updrafts. Only the ~6 km wide updraft at 1539:00 had a graupel-free core. Downwind of these updraft regions, the 2D-P concentrations increased to 11 $L^{-1}$ while the 2D-C measured about 140 $L^{-1}$ in the very turbulent area traversed between 1545:00 and 1553:00. The 2D-C concentration was much more variable than the 2D-P concentration.

The 2D-C images (Figs. 12 and 13) give good examples of the particles in these updrafts. As can be seen, the largest images are generally graupel. Outside these convective updrafts, the particle types are a mixture of graupel, snowflakes, and (occasionally) small needles or columns. The column forms are important because they are the only particles whose original crystal habit has not been obscured. Since these particles

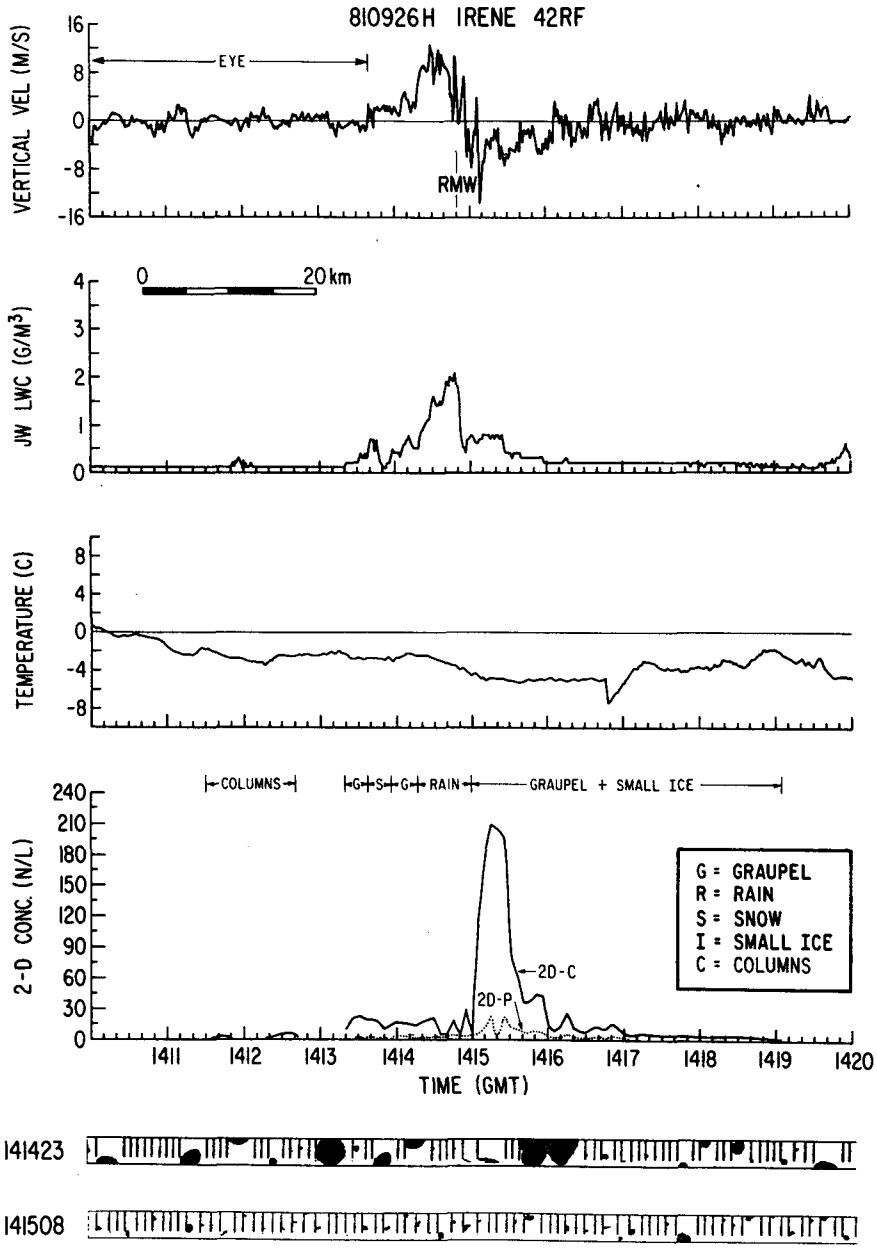


FIG. 11. As in Fig. 7 but for the radial traverse of the rainband of Hurricane Irene (26 September 1981).

were observed at −5°C, they are not likely to have fallen far below their original altitude, although they were certainly advected horizontally from their place of origin by the 50–60 m $s^{-1}$ tangential winds. These columns were observed from 1550 to 1552, about 60 km or more downwind from the major updraft that the aircraft encountered at 1544. However, since the aircraft encountered short-duration updrafts at 1549 and 1550, the flight path may have been on the edge of larger, stronger updrafts. It is conceivable that the smaller updrafts were the sources of the columns because ice particles are more likely to become heavily rimed in larger updrafts where there is more available cloud liquid water.

## 7. Discussion and synthesis

A synopsis of the vertical velocity, particle concentration, and JW liquid water content data collected in the updrafts and downdrafts from these three hurricanes is presented in Table 2. All of the data were gathered at altitudes above 5.0 km at temperatures between

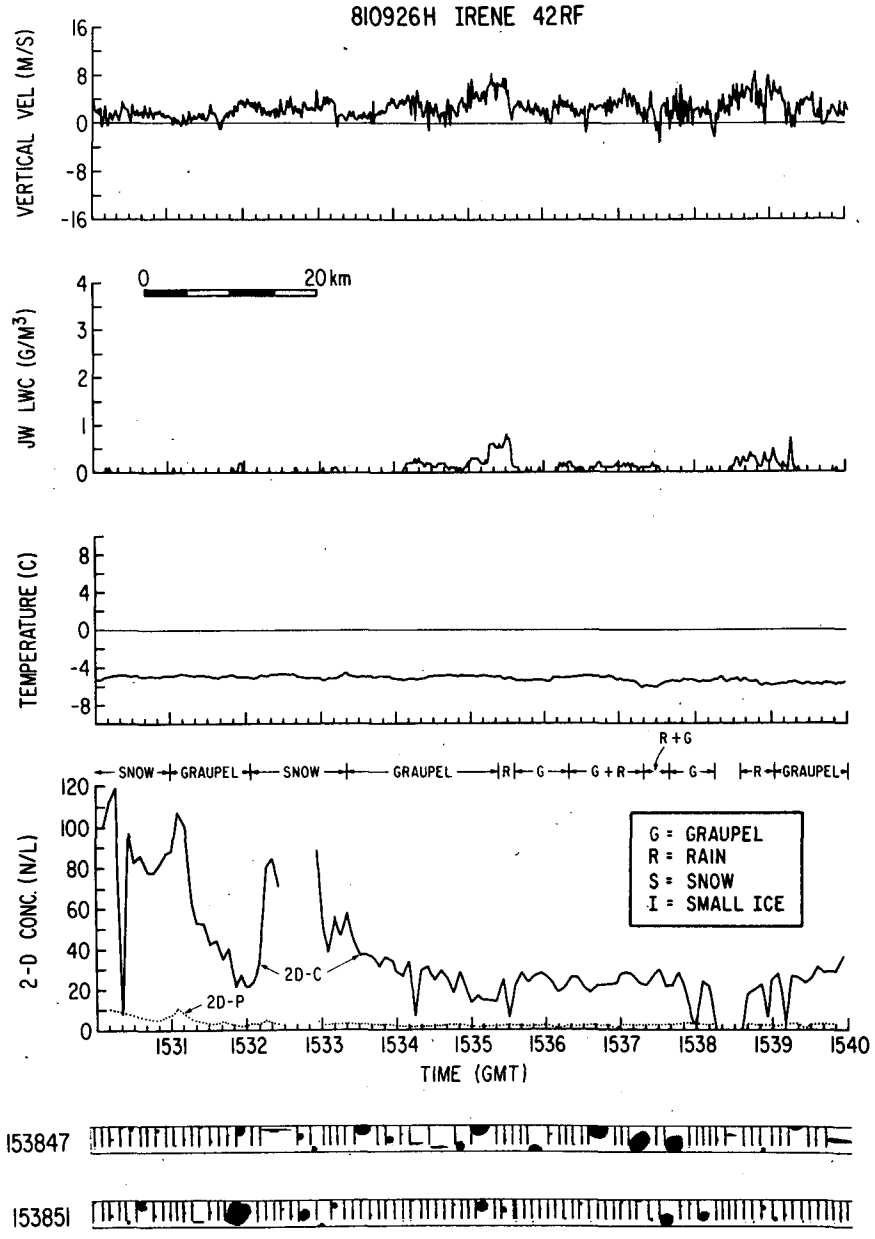


FIG. 12. As in Fig. 7 but for the circumnavigation of the Irene convective rainband. Note the elongated, canted image in the 1538:47 images.

−10 and +5°C. The data were stratified by storm, temperature, and JW liquid water content. Up and downdrafts were defined according to the criteria for updraft cores given by Jorgensen et al. (1985). Temperatures were average values within the updraft or downdraft, and the two columns at the far right refer to an average of the peak vertical velocities encountered in those updrafts that contain rain, and the number of updrafts in each category for which 2-D data were available. No 2-D data from Hurricane Ella were included in the table. The vertical velocity magnitudes given in the table represent the arithmetic means of the *peak* vertical velocities encountered in each up or downdraft in each category. Similarly, the JW lwc values also represent the arithmetic means of the peak JW lwc values observed in each updraft. The 2-D particle concentrations given are the arithmetic means of all 5.0 second average values computed for the up and downdrafts in each category. No rain was observed in downdrafts at temperatures below 0°C.

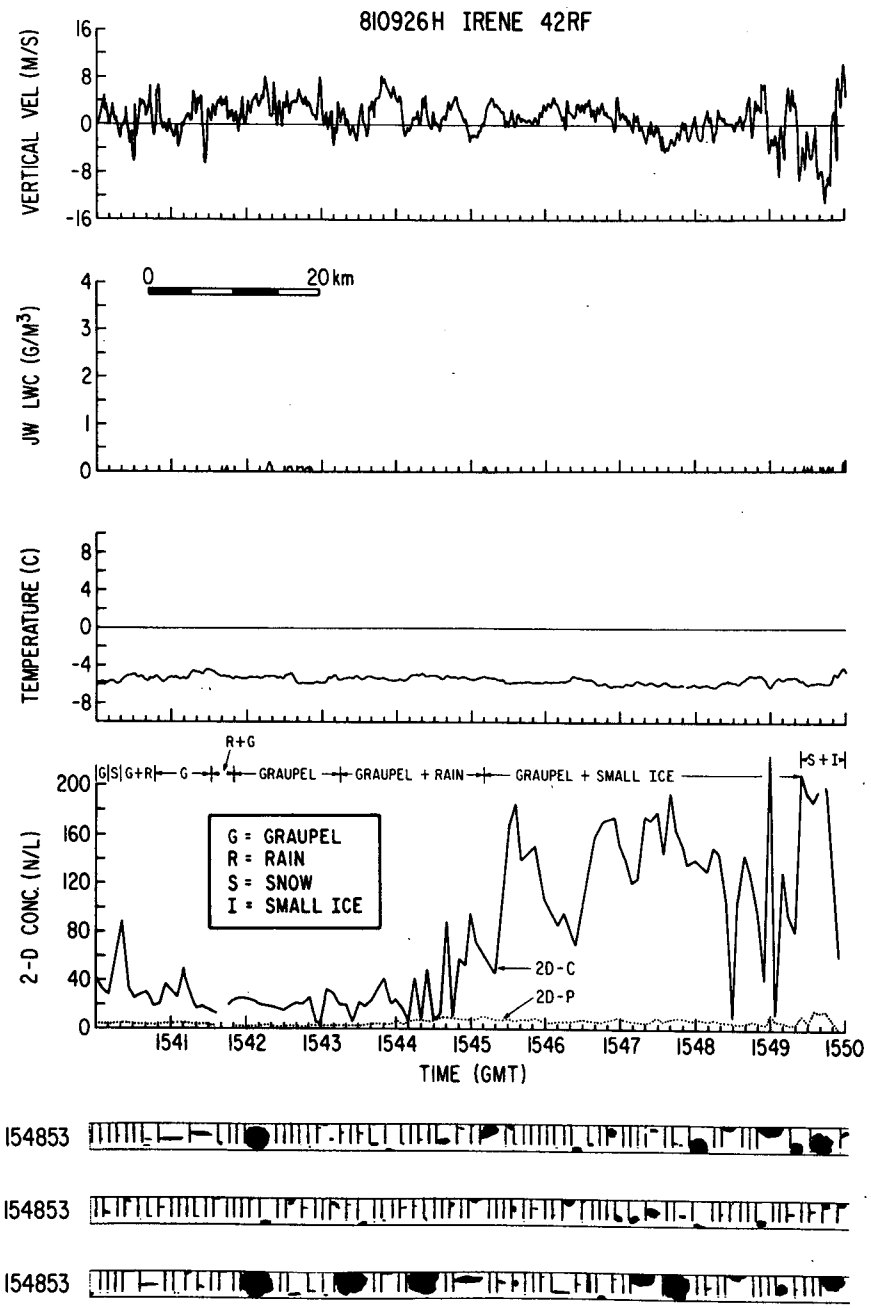


FIG. 13. As in Fig. 7 but for the end of the Irene circumnavigation.

At 6.0 km in these hurricanes, few distinct types of ice particles were observed that could be related directly to the temperatures at which the particles grew. Rather, particle type was more closely related to location relative to the convection. Table 2 clearly shows that supercooled rain is present at −5°C almost exclusively in updrafts stronger than 5 m $s^{-1}$, and that downdrafts usually contain more particles than updrafts. Most of the supercooled raindrops and cloud liquid water contents > 0.5 g $m^{-3}$ were found in the intense eyewall-like rainband of Irene. However, not all of the convective updraft cores encountered in these storms contain appreciable supercooled water. In convective updrafts with ice particle concentrations greater than 10–20 $L^{-1}$ at temperatures < 0°C, the observations suggest that the ice particles grow rapidly enough by vapor diffusion and riming at the expense of the cloud droplets to prevent the development of cloud liquid water contents > 0.5 g $m^{-3}$.

The work of Jorgensen (1984b) shows that in hurricane Allen, the mean radial flow above the 2 km level is outward from the eyewall, and below 2 km the mean flow is inward. Jorgensen also documented the outward radial slope of Allen's eyewall updraft. There is no reason to believe that other hurricanes are significantly different from Allen in this respect. Thus, ice particles that formed in the deep eyewall convection appeared to be injected into the mid- and upper level flow, where they could be distributed over the entire storm by the midlevel winds. The present dataset contained 20 radial passes at temperatures < −2°C. Fourteen updraft cores of >5 m $s^{-1}$ for >2 km were found, but only 4 of these were at temperatures < −2°C. In the convective rainband of Irene, over 1.5 hours of flight time were spent at the −5°C temperature level during tangential passes, and 20 updraft cores > 5 m $s^{-1}$ were encountered. The PMS data collected in stratiform precipitation is comprised of 3.5 hours of image data sampled in all parts of the hurricanes. Jorgensen et al. (1985) stratified updraft cores from several hurricanes by their vertical velocity, and compared them to updrafts measured for GATE and the Thunderstorm Project. In that study, the greatest one second integrated updraft speed in a region of continuous upward motion was defined as the peak updraft, and the mean updraft was the arithmetic mean of all the one second values in the same region. They found that a peak updraft at 6 km of 9 m $s^{-1}$ or more was stronger than 90% of the population of peak hurricane updrafts at that level. Similarly, a mean hurricane updraft of 4.7 m $s^{-1}$ is stronger than 90% of the population. Hurricane updrafts are much weaker than the corresponding continental thunder-

TABLE 2. A synopsis of the vertical velocity, JW liquid water content, and 2-D particle concentration data gathered in three Atlantic hurricanes.

| Category | Number up | $\overline{V_W}$ (m $s^{-1}$) | $\overline{JW_{max}}$ (g $m^{-3}$) | No. 2-D samples | Mean concentration ($L^{-1}$) 2D-P | 2D-C | $\overline{V_w}$ (m $s^{-1}$) (with rain) | Number of samples with rain |
|---|---|---|---|---|---|---|---|---|
| | | | *Updrafts** | | | | | |
| $T \leq -5$°C, JW > 0 g $m^{-3}$ | 150 | 4.0 | 0.3 | 57 | 5.8 | 37.8 | 8.4 | 22 |
| $T \leq -5$°C, JW ≥ 0.5 g $m^{-3}$ | 33 | 7.1 | 0.9 | 6 | 3.3 | 23.5 | 11.2 | 5 |
| −5°C < $T \leq -2$°C, JW > 0 | 116 | 4.1 | 0.5 | 46 | 4.1 | 15.9 | 7.3 | 16 |
| −5°C < $T \leq -2$°C, JW ≥ 0.5 g $m^{-3}$ | 34 | 7.4 | 0.9 | 16 | 4.1 | 16.8 | 9.8 | 7 |
| $T > -2$°C, JW > 0 g $m^{-3}$ | 84 | 3.5 | 0.3 | 41 | 4.7 | 13.2 | 6.4 | 33 |
| $T > -2$°C, JW ≥ 0.5 g $m^{-3}$ | 41 | 12.9 | 0.8 | 25 | 3.7 | 19.7 | 14.6 | 25 |
| $T \leq -5$°C, JW = 0 | 118 | 3.0 | 0 | 25 | 2.0 | 37.3 | 7.5 | 3 |
| −5 < $T \leq -2$°C, JW = 0 | 105 | 2.2 | 0 | 30 | 1.9 | 11.8 | 6.6 | 2 |
| $T > -2.0$°C, JW = 0 | 76 | 2.3 | 0 | 7 | 1.8 | 3.3 | 2.6 | 7 |
| | | | *Downdrafts*** | | | | | |
| $T \leq -5$°C | 24 | −3.6 | <0.1 | 13 | 8.9 | 76.7 | — | — |
| −5 < $T \leq -2$°C | 39 | −3.3 | <0.1 | 30 | 6.5 | 36.2 | — | — |
| $T > -2$°C | 83 | −2.7 | <0.1 | 17 | 3.2 | 15.1 | — | — |

* In columns 3 and 8 $\bar{V}_W$ and $\bar{V}_w$ are maximum in updrafts.
** In columns 3 and 8 $\bar{V}_W$ and $\bar{V}_w$ are minimum in downdrafts.

storm updrafts, and are similar in magnitude to the GATE updrafts. The statistics of Jorgensen et al. are representative of the convection sampled in this study since the vertical velocity data gathered during Allen is also included in their work.

The 10 m $s^{-1}$ updraft presented for the radial penetration of Irene occurred in the strong convective rainband and was one of the strongest updrafts in the entire dataset. The identification of graupel, even on the edge of an updraft of this magnitude at −2°C, is significant, because primary ice nucleation is ineffective at this temperature and secondary ice nucleation processes need some ice particles to work. This updraft was one of the few updrafts in the dataset to be completely free of graupel for a significant portion (about 33%) of its diameter, with little graupel for most of the rest of its diameter. At 50 kPa, the fallspeed of a 1 mm diameter water drop is about 5 m $s^{-1}$, and the updrafts are strongly tilted, so particles larger than about 1 mm fall out of the weaker updrafts rapidly. Given the observed updraft velocity distribution at 6 km and the large graupel present in almost all updrafts, there is little reason to expect large amounts of supercooled water at this altitude in these hurricanes. Thus, it is not surprising that little supercooled liquid precipitation was observed, except in the strongest updrafts of the hurricane eyewall. Moreover, the Irene circumnavigations showed that the lack of supercooled water at the −5°C level was real, not the result of poor sample statistics on the radial passes.

When one considers the quantity of ice found in hurricane convection, it is natural to attempt to determine its origin. Since ice nucleation from natural aerosols is not important at −5°C, a mechanism that can produce ice given the typical microphysical structure of maritime tropical cumulus clouds must be considered. The Hallett–Mossop secondary ice production process (Hallett and Mossop, 1974; Mossop and Hallett, 1974; Mossop, 1976, 1978; Foster and Hallett, 1982) is a possible mechanism. In this ice production process, small ice particles are shed from the surface of graupel growing in an updraft under a narrow range of conditions. This mechanism requires that the following conditions be met simultaneously:

(a) droplets < 13 um diameter with concentrations > ~100 $cm^{-3}$,

(b) droplets > 25 um diameter with concentrations > ~10 $cm^{-3}$,

(c) presence of millimeter-diameter graupel,

(d) temperature between −3 and −8°C, with the temperature of the peak particle production rate decreasing by 1°C for each additional gram per cubic meter of cloud liquid water content above 1 g $m^{-3}$, and

(e) the presence of >1.0 $L^{-1}$ of supercooled raindrops increases the rate of conversion of supercooled water to ice.

In the absence of direct evidence that the Hallett–Mossop conditions are met, the observation of graupel and columnar ice crystals near the active updrafts would constitute evidence that secondary ice particle production is taking place somewhere in the system, and implies the presence of some regions of supercooled cloud. The formvar replicator data gathered in Hurricane Ella provide the only direct evidence that the conditions favoring the Hallett–Mossop process were present in a hurricane. The cloud droplet spectra presented in Fig. 5 were recorded in a rainband outside the eyewall. They meet the Hallett–Mossop criteria for droplet spectra, as do many other formvar droplet spectra. In addition to the droplets, both the replicator and the 2D-C probes reveal the presence of both millimeter-sized graupel and columns. The FSSP data collected in Ella also indicate that cloud droplets existed at all diameters in its range (0.003–0.045 mm).

In the other two hurricanes, no direct confirmation of the existence of conditions suitable for secondary ice nucleation could be obtained, but indirect evidence, such as the discovery of millimeter graupel in all of the updrafts observed at temperatures colder than about −3°C, and the presence of columns in three of the downdrafts adjacent to the stronger updrafts (Ella at 1943:30, Allen 5 August at 1746:00, and Irene at 1415:30), is plentiful. The columns could only have been nucleated in the updraft near the −4°C level because only there were conditions favorable for column growth.

The radial penetrations showed that the ice particle concentration decreased rapidly with increasing distance from the convection. The ice particle concentration in Irene decreased from 40–200 $L^{-1}$ in the rainband to <0.1 $L^{-1}$ < 30 km or so radially outward. Hurricane Allen, with its vigorous eyewall, had a much thicker ice cloud in its outflow, as shown by the extensive stratiform areas visible on the radar composites. In Allen, the 2-D data revealed large aggregated snowflakes in concentrations that seldom fell below 1 $L^{-1}$ as far as 50 km radially outward from the eyewall. These data are clear indications that the eyewall convection was a major source of ice particles for the other parts of Allen because, particularly on 8 August 1980, the nearest rainband was 75 km or more beyond the eyewall. Given the relatively warm temperature at which this ice was found and given that most of the ice particles were graupel or snow, primary nucleation from atmospheric aerosol does not seem to have been the most likely ice-forming mechanism.

That secondary ice production involving graupel occurs in hurricanes was indicated by the repeated discovery of downdrafts warmer than −5°C which contained both graupel and numerous small ice particles, sometimes small columns. These downdrafts were always found adjacent to active updrafts, which provided a source of condensate. Most of the particles observed in the downdrafts had no recognizable crystal habit,

and particles large enough to be identified with a 0.050 mm resolution 2D-C probe (0.3–0.4 mm diameter) are also large enough to be efficiently rimed if supercooled cloud water is present. Thus any ice particles that were injected into the large updrafts would probably grow rapidly into graupel, so it is not surprising that we did not observe large numbers of small particles in the updraft regions. Because the cloud liquid water content (as measured by the JW device) in updrafts of comparable strength is much lower at temperatures < 0°C than at temperatures warmer than 0°C, most of the updrafts above the 0°C isotherm were probably glaciating.

The circumnavigation of Allen provides additional evidence in favor of rapid liquid to ice conversion in hurricanes. While Irene's rainband was similar to an eyewall, the rainband of Allen had an entirely different structure. It was primarily stratiform and almost totally glaciated, with only one updraft that exceeded 2 m $s^{-1}$. This updraft, which peaked at 6 m $s^{-1}$ at 1748:00, contained only graupel and numerous smaller ice particles. The JW liquid water content never exceeded 0.5 g $m^{-3}$, much less than was observed in updrafts of similar magnitude by the same JW on the same flight at temperatures > 0°C (see Fig. 8 for an example). Because the 2-D images were primarily medium-to-large graupel and snowflakes, most of the liquid water was concentrated in droplet sizes < 0.2–0.3 mm.

The observations from these three hurricanes have led to the development of a conceptual model of hurricane microphysics near the 0°C isotherm (Fig. 14). This model is based upon observations from the more than 10 radial penetrations of intense updrafts in eyewalls and rainbands, as well as four tangential traverses down the length of the convective rainband of Irene. The figure represents a typical composite of the 3.2 cm wavelength radar reflectivity cross-section through a convective eyewall containing a strong updraft–downdraft couplet, as well as typical variations of temperature, vertical velocity, and liquid water content. The dynamical features such as the radial wind, updraft slope, and the position of the tangential wind maximum are patterned after Jorgensen (1984b). Also presented are particle types and relative concentrations for both water and ice particles. The maximum reflectivity is associated with updrafts that contain <10 $L^{-1}$ raindrops and large graupel, while the downdraft on the outer edge of the reflectivity maximum contains large numbers of small ice particles. The downdrafts on the inner edge of the eyewall were observed on many occasions, particularly adjacent to strong updrafts. Ice particles were observed in the inner edge of the Irene radial penetration, but not in the others, probably because only the Irene pass was wholly colder than 0°C. The closer the penetration is to the altitude of the 0°C isotherm in the outer regions, the sharper the transition is between liquid and ice particle areas between the up- and downdrafts. Cloud liquid water contents > 1 g

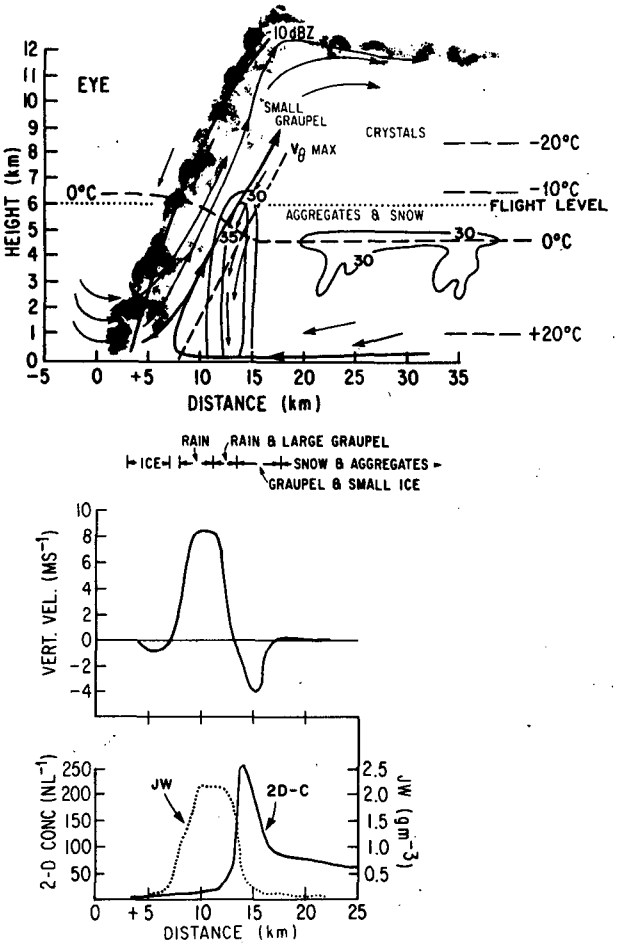


FIG. 14. Schematic of the strong eyewall updraft-downdraft in radial cross section, showing the location of the updraft with respect to the eyewall and principle rainband. The concentration and particle phase indications represent what would be typically found in a penetration across such a feature at a level at or <2 km above the altitude of the melting level in the outer regions of the storm. Ice particles on the inner edge of the convection were only found in the radial penetration of the Irene rainband. That penetration was the only one made where the inner edge was colder than 0°C.

$m^{-3}$ occur only in updrafts warmer than −1°C or stronger than about 5 m $s^{-1}$, which implies a rapid conversion of cloud water to ice. The sharp horizontal temperature gradient present in the eyewall provides a path whereby ice particles may be transported very near the level of the 0°C isotherm in the updraft. This temperature gradient is often >0.5°C $km^{-1}$, and allows downdrafts to advect much ice to levels where it can be mixed into the updrafts by turbulent mixing, thus allowing both graupel production and secondary nucleation of new ice particles to proceed in a self-sustaining manner.

The eyewall penetrations without strong updrafts or downdrafts were quite different than the others. These weak updrafts in eyewalls never contained >0.5 g $m^{-3}$ of JW liquid water above the 0°C isotherm level, and

the ice particle concentrations in the outer portions of them were >30–50 $L^{-1}$. The updrafts were generally too weak to support millimeter droplets, the cloud droplets responsible for the JW liquid water content are too small for the NOAA 2D-C to measure, and the penetration temperatures were usually too warm (about −1°C) for efficient ice nucleation. The relatively flat size spectra suggest that the ice particles were advected horizontally, and did not nucleate where they were observed. Furthermore, the low liquid water contents and low updraft velocities are not conducive to graupel growth or secondary ice production.

The occurrence of downdrafts on the eye side of the eyewall points to a region of substantial mixing between the saturated air of the eyewall and the dry subsiding air of the eye. This mixing alone can give rise to appreciable negative buoyancy, and could be responsible for the observed downdrafts. More importantly, the evaporatively cooled air could descend within the sloping eyewall itself, to mix ice particles downward into the adjacent updraft. The mixing thus appears to be the reason that supercooled water fails to penetrate to heights much above the −5°C level in hurricane eyewalls; downdrafts sheath *both* sides of the updraft, leading to strong shear regions and ice incorporation.

Stratiform areas are much different from the eyewalls in that the medium and large particles are primarily aggregated snowflakes. Columns, if present in the stratiform regions, were almost always observed within 10–15 km of convective updrafts. The stratiform regions were characterized by the almost total absence of cloud and precipitation-sized liquid water. Ice particle concentrations were generally 5–25 $L^{-1}$, and the particle size spectra were flat, which indicates that the nucleation and advection of small ice into this region was balanced by the aggregation and sedimentation of ice out of this area.

## 8. Summary and conclusions

This paper reports observations of the phase, concentration and spatial distribution of cloud and precipitation particles above the 0°C isotherm in three Atlantic hurricanes. The observations indicate that except in the strongest updrafts, hurricane convection is largely glaciated at temperatures as warm as −5°C. Furthermore, most hurricane updrafts contain at least some graupel, even at temperatures as warm as −2°C, and all updrafts > 5 m $s^{-1}$ existed in close proximity to downdrafts that contained large concentrations of ice particles. Total particle concentrations as high as 200 $L^{-1}$, of which 20–30 $L^{-1}$ were graupel, occurred frequently in downdrafts. Many of the smaller particles were columnlike, indicating ice grown by diffusion at a temperature near −4°C. Outside the updraft/downdraft areas, the particles were primarily large snowflakes and some columns with concentrations of 15–30 $L^{-1}$ in rainbands, and 1–15 $L^{-1}$ between the eyewall and principal rainband. No cloud liquid water or liquid precipitation was observed above the melting level in any stratiform area except in the updraft in Allen's principal rainband.

The presence of ice both in the convective and stratiform areas lends credence to the numerical results obtained by Lord et al. (1984) using an axisymmetric hurricane model with parameterized ice microphysics. Extensive mesoscale downdrafts that originated near the 0°C isotherm occur in the model. The mesoscale downdrafts substantially slowed the growth of the model vortex in comparison with model runs without the ice microphysics. The relative abundance of fast-falling graupel with respect to slow-falling snow controlled the horizontal spread of the cooling caused by melting particles. Thus, the locations of the mesoscale downdrafts were controlled by ice particles.

Radar observations provided indirect confirmation of the presence of ice. The rainband and eyewall radar reflectivity decreased very rapidly with height above the 0°C isotherm, and a brightband was often observed below the 0°C isotherm in the rainbands (Jorgensen, 1984a). These observations lead to the speculation that most of the liquid water that reaches the 0°C isotherm in hurricanes is frozen well below the −10°C isotherm. This is in direct contrast to the situation over southern Florida in summer, where ice particles were relatively rare at −10°C in natural growing convective clouds (Hallett et al., 1978). The warm temperatures involved in this study, plus the abundant graupel in hurricane convection argue against the predominance of primary nucleation as the principal ice-forming mechanism. Rather, most of the ice originates through secondary nucleation or "ice multiplication" processes in the eyewall updrafts. This ice is redistributed throughout the storm by the upper and midlevel outflows. The redistribution results in ice concentrations in the stratiform areas that are much larger than those which could be generated by primary nucleation alone. An important deduction can be made from these results.

The presence of supercooled water is evidence for a microphysically unstable cloud system. In these hurricanes, little supercooled water was observed anywhere except in the strongest eyewall updrafts. Thus, given the apparent scarcity and transient nature of these updrafts, as well as the vast quantities of ice particles at the 6 km level in all quadrants of the storm, it is unlikely that large quantities of supercooled water reach temperatures colder than about −10°C in mature hurricanes. Active cloud seeding with ice nuclei in mature hurricanes, as had been attempted in project STORMFURY, would seem to be superfluous (Willoughby et al., 1985).

Nevertheless, developing tropical storms that do not have a closed circulation above the 0°C level may occasionally contain sufficient supercooled water for cloud seeding with ice nucleants to be effective. The simultaneous occurrence of supercooled water and ice

that was occasionally observed in the eyewall has been shown to be related to electric charge separation (Dye et al., 1986). This evidence suggests that remote measurements of lightning or electric field strength may be useful in locating regions in the hurricane that contain supercooled liquid water. The transient occurrence of supercooled water associated, for example, with eyewall regeneration (Jorgenson, 1984b) should also be considered. Glaciation of such regions may occasionally be delayed enough to allow the penetration of supercooled water to higher, colder levels, as often occurs in isolated cumulus convection. However, the first updraft to glaciate in this situation would eventually supply ice to be transported both radially and tangentially around the storm (within about 30 min) to naturally seed any remaining supercooled water.

*Acknowledgments.* We would like to thank the many people whose help and encouragement were instrumental in producing this paper. The advice and constructive criticism of the manuscript given by Drs. Robert Burpee, Hugh Willoughby, and David Jorgensen greatly contributed to the completion of this work. Figure 14 was developed through many discussions of hurricane dynamics with Drs. Frank Marks, David Jorgensen, and Robert A. Houze, Jr. Constance Arnhols gave much editorial assistance and the figures were expertly drafted by Dale Martin and David Senn. J.H. was supported in part by National Science Foundation, Meteorology Program, Grant ATM 8218349.

## REFERENCES

Ackerman, B., 1963: Some observations of water contents of hurricanes. *J. Atmos. Sci.*, **20,** 288–298.

Churchill, D. D., and R. A. Houze, Jr., 1984: Development and structure of winter monsoon cloud clusters on 10 December 1978. *J. Atmos. Sci.*, **41,** 933–960.

Dye, J. E., J. J. Jones, W. P. Winn, T. A. Cerni, Barry B. Gardiner, D. Lamb, R. L. Pitter, J. Hallet and C. P. R. Saunders, 1986: Early electrification and precipitation development in a small, isolated Montana cumulonimbus. *J. Geophys. Res.*, (in press).

Foster, T., and J. Hallett, 1982: A laboratory investigation of the influence of liquid water content on the temperature dependence of secondary ice crystal production during soft hail growth. *Preprints, Conf. on Cloud Physics,* Chicago, Amer. Meteor. Soc. 123–126.

Hallet, J., 1976: Measurements of the size, concentration and structure of atmospheric particulates by the airborne continuous replicator. Final Rep., Cloud particle replicator for use on a pressurized aircraft, 92 pp; Parts I, II, Supplementary Final Report, 151 pp. Contract No. AFGL-TR-76-1149.

——, and S. C. Mossop, 1974: Production of secondary ice particles during the riming process. *Nature,* **249,** 26–28.

——, R. I. Sax, D. Lamb and A. S. R. Murty, 1978: Aircraft measurements of ice in Florida cumuli. *Quart. J. Roy. Meteor. Soc.,* **104,** 631–651.

Heymsfield, A. J., C. A. Knight and J. E. Dye, 1979: Ice initiation in unmixed updraft cores in NE Colorado cumulus congestus. *J. Atmos. Sci.*, **36,** 2216–2229.

Jorgensen, D. P., 1984a: Mesoscale and convective-scale characteristics of mature hurricanes. Part 1: General observations by research aircraft. *J. Atmos. Sci.*, **41,** 1268–1285.

——, 1984b: Mesoscale and convective-scale characteristics of mature hurricanes. Part 2: Inner core structure of Hurricane Allen (1980). *J. Atmos. Sci.*, **41,** 1287–1311.

——, and P. T. Willis, 1982:A *Z–R* relationship for hurricanes. *J. Appl. Meteor.*, **21,** 35—366.

——, E. J. Zipser and M. A. LeMone, 1985: Vertical motions in intense hurricanes. *J. Atmos. Sci.*, **42,** 839–856.

Keller, V. W., and R. I. Sax, 1981: Microphysical development of a pulsating cumulus tower: A case study. *Quart. J. Roy. Meteor. Soc.*, **107,** 679–697.

Knollenberg, R. G., 1981: Techniques for probing cloud microstructure. *Clouds, Their Optical Properties and Effects.* P. V. Hobbs and A. Deepak, Eds., Academic Press, 15–89.

Lawrence, M. B., 1979: Atlantic hurricane season of 1978. *Mon. Wea. Rev.*, **107,** 477–491.

——, and J. M. Pelissier, 1981: Atlantic hurricane season of 1980. *Mon. Wea. Rev.*, **109,** 1567–1582.

Lenschow, D. H., and W. T. Pennell, 1974: On the measurement of in-cloud and wet-bulb temperatures from an aircraft. *Mon. Wea. Rev.*, **102,** 447–454.

Lord, S. J., H. E. Willoughby and J. M. Piotrowicz, 1984: Role of a parameterized ice-phase microphysics in an axisymmetric, nonhydrostatic tropical cyclone model. *J. Atmos. Sci.*, **41,** 2836–2848.

Marks, F. D. Jr., 1985: Evolution of the structure of precipitation in Hurricane Allen. *Mon. Wea. Rev.*, **113,** 909–930.

Mossop, S. C., 1976: Production of secondary ice particles during the growth of graupel by riming. *Quart. J. Roy. Meteor. Soc.*, **102,** 45–57.

——, 1978: The influence of drop size distribution on the production of secondary ice particles during graupel growth. *Quart. J. Roy. Meteor. Soc.*, **104,** 323–330.

——, and J. Hallett, 1974: Ice crystal concentration in cumulus clouds: Influence of the drop spectrum. *Science,* **186,** 632–634.

Pruppacher, H. R., and J. D. Klett, 1978: *Microphysics of Clouds and Precipitation.* Reidel, 714 pp.

Willoughby, H. E., J. A. Clos and M. G. Shoreibah, 1982: Concentric eyewalls, secondary wind maxima, and the evolution of the hurricane vortex. *J. Atmos. Sci.*, **39,** 395–411.

——, F. D. Marks and R. J. Feinberg, 1984: Stationary and moving convective bands in hurricanes. *J. Atmos. Sci.*, **41,** 3189–3211.

——, D. P. Jorgensen, R. A. Black and S. L. Rosenthal, 1985: Project STORMFURY: A scientific chronicle 1962 to 1983. *Bull. Amer. Meteor. Soc.*, **66,** 505–514.